Recursive Updates of Wildfire Perimeters Using Barrier Points and Ensemble Kalman Filtering

Abhishek Subramanian[1], Li Tan[1], Raymond A. de Callafon[1(✉)], Daniel Crawl[2], and Ilkay Altintas[2]

[1] Department of Mechanical and Aerospace Engineering, University of California San Diego, La Jolla, CA, USA
{absubram,ltan,callafon}@eng.ucsd.edu
[2] San Diego Supercomputer Center, University of California San Diego, La Jolla, CA, USA
{crawl,altintas}@sdsc.edu

Abstract. This paper shows how the wildfire simulation tool FARSITE is augmented with data assimilation capabilities that exploit the notion of barrier points and a constraint-point ensemble Kalman filtering to update wildfire perimeter predictions. Based on observations of the actual fire perimeter, stationary points on the fire perimeter are identified as barrier points and combined with a recursive update of the initial fire perimeter. It is shown that the combination of barrier point identification and using the barrier points as constraints in the ensemble Kalman filter gives a significant improvement in the forward prediction of the fire perimeter. The results are illustrated on the use case of the 2016 Sandfire that burned in the Angeles National Forest, east of the Santa Clarita Valley in Los Angeles County, California.

Keywords: Wildfire · Barrier points · Ensembles · Ensemble Kalman filter · FARSITE

1 Introduction

The ability to reliably predict fire perimeter propagation during a wildfire event has a large potential in resource allocation and fire fighting planning to help save lives and valuable infrastructure. Studying wildfire dynamics is done by collecting data [3] and combining wildfire simulation tools with experimental data to assimilate or adjust the widfire simulation [11–14]. Previous work on data assimilation using the FARSITE [7] wildfire simulation tool combined with ensemble Kalman filtering can be found in [5,16]. Next to large body of work that use some form of Kalman filtering, [2,4,8,10] there are alternative approaches

This work was partly funded by NSF 1331615 under CI, Information Technology Research and SEES Hazards programs.

V. V. Krzhizhanovskaya et al. (Eds.): ICCS 2020, LNCS 12142, pp. 225–236, 2020.
https://doi.org/10.1007/978-3-030-50433-5_18

that use Genetic Algorithms to determine the best set of input parameters to match the measurements [1]. The power of a data driven approach is also confirmed by [17] illustrating improvements to wildfire prediction on data obtained from physical experiments.

Fire perimeters that may be obtained periodically during a wildfire event may be well-suited for periodic or recursive updates of the initial conditions (e.g. initial fire perimeter) and the relevant parameters that govern the wildfire dynamics. For a Kalman filter-based approach it is essential that wildfire perimeter measurements are quantified with a measurement accuracy to find the optimal trade-off in adjusting initial conditions and wildfire parameters. To this extend, the work by [14] uses thermal-infrared imaging to measure the true fire perimeter on a controlled fire experiment done on a $(4\,\mathrm{m} \times 4\,\mathrm{m})$ patch of land and [17] used ForeFire/Meso-NH simulations produced by [6] as observations. Unfortunately, such methods cannot be employed for time-sensitive and large scale wildfires, where perimeters are obtained with aerial measurements and computations of future wildfire perimeters must be done in near real-time.

To improve the quality of wildfire prediction and to speed up computations, one piece of critical information is often neglected in wildfire data assimilation: stationary points at which a (part of the) fire perimeter remains at the same locations between periodic updates. Clearly, those points can be characterized with a relatively high accuracy and do not require computational updates. In terms of data assimilation, such stationary points can be viewed as constrains in a constrained Ensemble Kalman Filtering [15] formulation. Fortunately, the FARSITE [7] wildfire simulation tool has the notion of barrier points to account for stationary fire perimeters. Identifying such stationary or barrier points on the fire perimeter and combining this information with ensemble Kalman filtering is the main contribution of this paper.

The results presented are based on the work in [5,16] to fully use the information of barrier points in the prediction and update steps of the data assimilation tools for FARSITE. The approach presented in this paper performs recursive data assimilation to estimate the true values of fuel dependent adjustment factors along with wind speed and direction that influence fire spread rate by including them in the state updates. Estimation of these input parameters along with the identification of barrier points further improve the periodic prediction of fire perimeters. The data assimilation tools are tested on actual wildfire perimeter data that was obtained for the 2016 Sandfire that burned in the Angeles National Forest, east of the Santa Clarita Valley in Los Angeles County, California.

2 Contour and Stationary Points

2.1 Fourier Analysis

To introduce the concept of stationary points, we first formalize the approximation of a fire perimeter as a n-polygon described by a ordered sequence of n piece-wise linear line segments parametrized in Eastern e_j and Northern n_j

coordinate pairs (e_j, n_j), $j = 0, 1, \ldots, n-1$. To simplify notation, we may represent the n coordinates of the n-polygon as a complex number $p_j = e_j + i \cdot n_j$ for which we can define a complex Discrete Fourier Transform (DFT)

$$u_l = \sum_{j=0}^{n-1} p_j e^{-il\frac{2\pi}{n}j} \tag{1}$$

and represent the fire perimeter p_j, $k = 0, 1, \ldots, n-1$ by the complex sequence Fourier series u_l, $l = 0, 1, \ldots, n-1$. Since a fire perimeter is always a closed polygon, e.g. p_1 is connected to p_n via a linear line segment, the parametrization of the n-polygon should be independent of the starting point p_1 and the (anti)clock wise rotation of the sequence p_j in the complex plane. A shift in the starting point or rotation can be easily represented in the Fourier series $\bar{u}_l$ by an additional phase shift of u_l and given by $\bar{u}_l = u_l e^{-i\phi}$, where the rotation angle ϕ is determined by an integer shift in the starting point and the binary choice on the anti-clockwise or clockwise rotation of p_j [9]. The Fourier series representation u_l of the n-polygon approximation of a fire perimeter allows fire perimeters at subsequent time steps k and $k+1$ to be compared as parts of the fire perimeter might be stationary. A non-moving or stationary part of the fire perimeter may be due to the presence of a nonburnable surface fuel or explicit fire fighting efforts in which part of the surface fuel has been removed or extinguished. Such information must be taken into account to improve the prediction of fire perimeter progression over time.

To identify stationary parts of the fire perimeter, we consider fire perimeters represented by the n-polygon $p_j(k)$, $j = 0, 1, \ldots, n-1$ at time step k and a m-polygon $p_j(k+1)$, $j = 0, 1, \ldots, m-1$ at a subsequent time step $k+1$. As $n \neq m$ and the starting point $p_1(k) \neq p_1(k+1)$, the simple check of $p_j(k) = p_j(k+1)$ will not suffice in determining the stationary points $p_j(k)$ of the fire perimeter. Instead, we first consider the Least Squares minimization

$$\bar{\phi} = \arg\min_{\phi} \sum_{l=0}^{d-1} |u_l(k) - u_l(k+1)e^{-i\phi}|^2 \tag{2}$$

where $d = \min(m, n)$ and $u_l(k)$, $u_l(k+1)$ are given by the DFT in (1). The optimization in (2) recomputes the optimal starting point and rotation of the Fourier transform of the m-polynomial $p_j(k+1)$ by evaluating the difference between $s = \min(m, n)$ Fourier coefficients. The end result is a set of Fourier coefficients $\bar{u}_l(k+1) = u_j(k+1)e^{-i\bar{\phi}}$ for which the inverse DFT will lead to a re-oriented m-polygon $\bar{p}_j(k+1)$, $j = 0, 1, \ldots, m-1$ of the fire perimeter at time step $k+1$ that can be compared with the fire perimeter $p_j(k)$, $k = 0, 1, \ldots, n-1$ at time step k. Stationary points are now defined as the set of points $p_j(k) \in \mathcal{P}_k$ on the fire perimeter $p_j(k)$ at time step k for which

$$\mathcal{P}_k : |p_j(k) - \bar{p}_j(k+1)| \leq \varepsilon \text{ for } k = t, t+1, \ldots, t+t_{stat}-1, \quad t = 0, 1, \ldots, d-t_{stat} \tag{3}$$

where $t_{stat} > 1$ ensures no single points for which $|p_j(k) - \bar{p}_j(k+1)| \leq \varepsilon$ are identified as stationary points. Only a sequence of t_{stat} points on the fire perimeter $p_j(k)$ at time step k and $\bar{p}_j(k+1)$ at time step $k+1$ must lie within a distance of ε to qualify as stationary points.

2.2 Illustration and Boundary Points

The above proposed identification of stationary points is illustrated in Fig. 1, that shows fire perimeter measurements for two consecutive (time step $k = 0$ and time step $k = 1$) for the use case of the 2016 Sandfire that burned in the Angeles National Forest, east of the Santa Clarita Valley in Los Angeles County, California. It can be seen that only the lower portion of the fire has propagated from time step $k = 0$ to $k = 1$, indicating a large set of stationary points in the progression of ther wildfire.

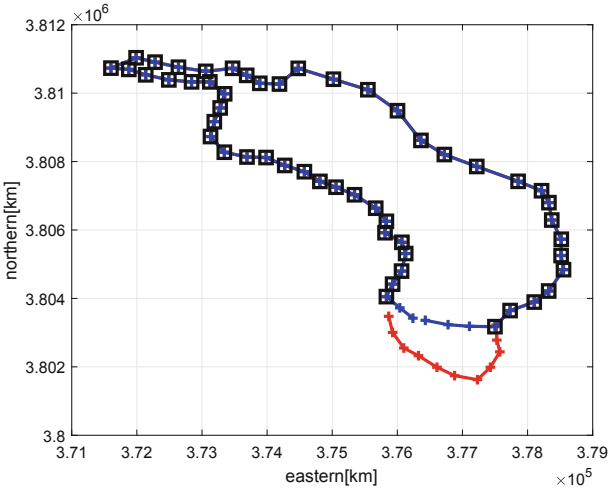

Fig. 1. Polygon approximation of fire perimeter measurement at time step k = 0 (blue) compared with the fire perimeter at the subsequent time step $k = 1$ (red) for the 2016 Sandfire. Black squares are the identified stationary points of the fire perimeter at time step $k = 0$. (Color figure online)

With the re-orientation of the fire perimeter points found by the optimization in (2), the location of stationary points identified by the black squares in Fig. 1 become apparent. It should be noted that stationary points along the fire perimeter might persist only for certain amount of time, as the fire could eventually progress. For example, the stationary points shown in Fig. 1 are only valid for the fire perimeter at time step $k = 0$. To identify the stationary points for the fire perimeter at $k = 1$, measurement at time step $k = 2$ are required. Clearly, the information on the set of stationary points is important in predicting the

spread of wildfires accurately. The wildfire simulation tool FARSITE [7] has the notion of a barrier perimeter defined by barrier points to account for the identified stationary points in the fire perimeter by temporarily defining surface fuels as non-burnable.

3 Data Assimilation

3.1 Ensemble Forward Simulation

The FARSITE wild fire simulation tool takes in n real valued eastern- and northern-coordinates of a fire perimeter $p_j(k)$ at time step k to simulate a fire perimeter $p_j(k+1)$ at time step $k+1$. Next to the initial perimeter $p_j(k)$ specified in a shape file, FARSITE also uses information on surface fuels, topography, wind speed, wind direction and fuel adjustment factors, collectively combined in the environmental parameter θ_k at time step k, to adjust the fire perimeter prediction [16]. In addition, FARSITE can account for a set of barrier points $b_j(k) \in \mathcal{P}_k$ as defined in (3) to approximate the stationary points of the fire perimeter. Using only real valued calculations, FARSITE can be viewed as a non-linear mapping

$$X(k+1) = f(X(k), \theta_k, B_k) \tag{4}$$

where $X(k)$ is a vector of the eastern- and northern coordinates of the wild fire perimeter $p_j(k)$ and B_k is a vector of the eastern- and northern coordinates of the barrier points $b_j(k)$.

It should be noted that the non-linear map $f(\cdot)$ is not known analytically and both sensitivity or uncertainty of the inputs $X(k)$, θ_k and B_k can be evaluated numerically via ensemble averaging. For that purpose, random samples (ensembles) are chosen from a probability description of the initial fire perimeter $X(k)$ and possibly the environmental parameters θ_k. In this paper only uncertainty on the initial fire perimeter $X(k)$ is considered in the form of a covariance on the vector $X(k)$, whereas the environmental parameters θ_k and the barrier points B_k are assumed to be fixed. The later is a reasonable assumption as barrier points are defined as stationary points, whereas variability in θ_k can be considered as a possible improvement for the ensemble forward simulation presented in this paper.

The approach of ensemble forward simulation is similar to presented earlier in [16], but with the important addition of the vector of barrier points B_k. For the initialization of the covariance matrix P_k on the vector $X(k)$ for fire perimeter points, the proximity of the eastern- and northern-coordinates to its neighboring points is used. The proximity measure for the covariance σ_{e_j,n_j} for each point (e_j, n_j) on the n-polygon of the fire perimeter is defined by $\sigma_{e_j,n_j} = h(e_{j-1}, y_{j-1}, e_j, n_j, e_{j+1}, n_{j+1})$, where $h(\cdot)$ is a function that computes the measure of closeness of each point to its neighboring points on the fire perimeter. The value of σ_{e_j,e_j} is inversely proportional to the distance of (e_j, n_j) with its neighboring points. Using the environmental parameters θ_k, barrier points B_k and N ensembles $X^i(k)$ taken from a normal distribution determined by the

mean value $X(k)$ and the covariance σ_{e_j,n_j}, each ensemble member $X^i(k)$ at time step k is advanced through the forward model

$$X^i(k+1) = f(X^i(k), \theta_k, B_k), \quad i = 1, 2, \ldots, N,$$

where B_k is determined *recursively* from a measurement of a fire perimeter $X(k+1)$ at time step $k+1$ by the optimization in (2) and the definition of the stationary points in (3) using the mean value $X(k)$.

With the ensemble forward simulation, N predicted fire perimeters $X^i(k+1)$ or $p_j^i(k+1)$ for $i = 1, 2, \ldots, N$ and $j = 0, 1, \ldots, n_i$ have become available. For ensemble averaging, a mean value and a covariance must be estimated, but typically two different fire perimeter boundaries $X^i(k+1)$ and $X^j(k+1)$ will not have the same number n_i of polygon points, starting point of orientation. To address this issue, first all N predicted fire perimeters $p_j^i(k+1)$, $i = 1, 2, \ldots, N$ are interpolated to the same number of (maximum) points $n_{max} = \max_i(n_i)$. Subsequently, an optimization similar to (2) is performed to align the starting point and orientation of all the ensembles. Denoting $u_l^1(k+1)$ as the DFT transform of the first (primary) ensemble $p_j^1(k+1)$ for $j, l = 0, 1, \ldots, n_{max}$, the other ensembles are aligned using the minimization

$$\bar{\phi}^i = \arg\min_{\phi} \sum_{l=0}^{n_{max}-1} |u_l^1(k+1) - u_l^i(k+1)e^{-i\phi}|^2, \tag{5}$$

for the index $i = 2, \ldots, N$, while i in the exponent $e^{-i\phi}$ still denotes the complex number $i^2 = -1$. The $N-1$ optimizations in (5) leads to a re-oriented set of ensembles represented by the vector $\bar{X}^i(k+1)$ for $i = 2, \ldots, N$ and found by the inverse DFT of $\bar{p}_j^i(k+1) = u_l^i(k+1)e^{-i\phi^i}$. The end result of this process is set of properly aligned N ensembles $X^1(k+1)$ and $\bar{X}^i(k+1)$, $i = 2, \ldots, n$ for which a mean $X^\mu(k+1) \in \mathcal{R}^{n_{max}}$ and a covariance $P^\mu(k+1) \in \mathcal{R}^{n_{max},n_{max}}$ can be computed.

3.2 Ensemble Kalman Filter Update

In the ensemble Kalman filter update, a measurement of a fire perimeter obtained at time step $k+1$ is consolidated with the prediction of the mean $X^\mu(k+1) \in \mathcal{R}^{n_{max}}$ and the covariance $P^\mu(k+1) \in \mathcal{R}^{n_{max},n_{max}}$ obtained from the ensemble forward simulation described above. For the optimal consolidation of the measurement and the prediction, we assume that the fire perimeter obtained at time step $k+1$ is described by its mean $Y(k+1)$ and a covariance $P^y(k+1)$. It is worth noting that the covariance $P^y(k+1)$ may be determined by either the inherent limited accuracy in obtaining the measurement $Y(k+1)$, the relative distance between the points on the perimeter $Y(k)$ or estimated by computing a two-dimensional variance from multiple measurements [5].

As the points of the measured fire perimeter $Y(k+1) \in \mathcal{R}^m$ and typically $m \neq n_{max}$, the different size of the observation and prediction is handled by linear interpolation of $Y(k+1)$ and $P^y(k+1)$ to n_{max} points. Subsequently, the following steps are done for each ensemble pair contained in $\tilde{X}$ and $\tilde{Y}$.

1. Find the closest point on $\tilde{X}^e$ to each point in $\tilde{Y}^e$ and pair them up, store the pair for which magnitude of distance is minimum and discard others, i.e. capture i that satisfies,

$$\min_i(\min_j |y_i^e - x_j^e|) \quad \forall i = 1, ..., m/m_i$$
$$j = \{1, 2, ..., n_{max}\}/m_j$$

along with i store its corresponding j in m_i and m_j respectively
2. Repeat the step above until each point in $\tilde{Y}^e$ is paired with a unique point in $\tilde{X}^e$.
3. This pairing scheme is used to construct the C matrix that is required to perform the Kalman update step to get the updated perimeter using the Kalman gain K via

$$X^e_{updated} = \tilde{X}^e + K[\tilde{Y}^e - C\tilde{X}^e] \tag{6}$$

The steps above are repeated until all ensembles have been exhausted. In this manner we perform data assimilation to improve our prediction by optimally combining results from a forward model (with errors in input) and measurement (with errors). Incorporation of stationary point information in the form of the barrier points B_k is done in the forward model itself to improve the ensemble forward simulation.

4 Results for the 2016 Sand Fire

4.1 Illustration for Single Step Data Assimilation

For the illustration of the data assimilation with barrier points, ensemble forward simulations and actual measurements of the 2016 Sandfire in Los Angeles County, California are used at time steps k separated by 2 h intervals, as shown in Fig. 2.

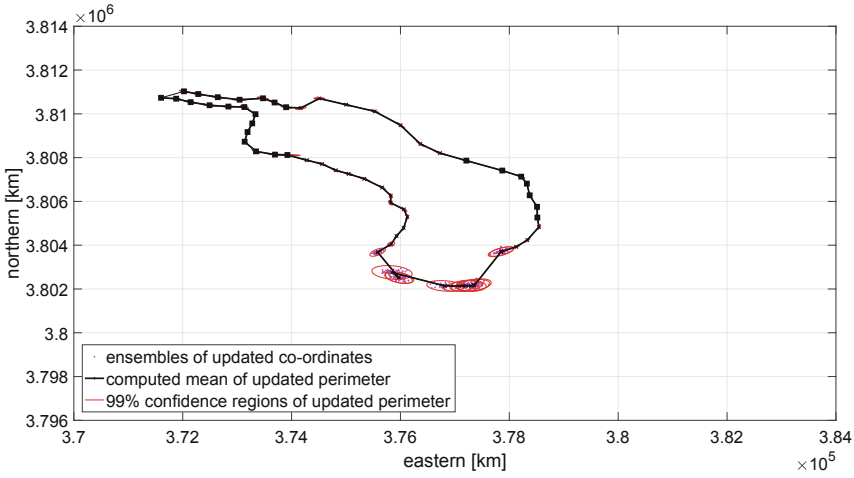

Fig. 2. Initial fire perimeter at time step $k = 1$.

In this case, the input fire perimeter given to FARSITE at step $k = 1$ shown in Fig. 2 is obtained from ensembles of the last fire perimeter depicted earlier in Fig. 1. Note that the variability along the fire perimeter at step $k = 1$ is very small and virtually non-existent in certain parts due to the stationary points identified from the previous time step at $k = 0$.

The stationary points for the fire perimeter at time step $k = 1$ are indicated by the black squares in Fig. 2. The stationary points are found by the procedure outlined earlier in Sect. 2 using the interpolated fire perimeter $X(k+1)$ obtained from a measurement of the actual fire perimeter $Y(k+1)$ at time step $k+1 = 2$. With the identified stationary points, barrier perimeters are defined in FARSITE and the ensemble forward simulation now lead to a predicted fire perimeter characterized by a mean $X^{\mu}(k+1) \in \mathcal{R}^{n_{max}}$ and a covariance $P^{\mu}(k+1) \in \mathcal{R}^{n_{max},n_{max}}$ as described earlier in Sect. 3.1. A comparison of the measurement of the actual fire perimeter $Y(k+1)$ and the predicted mean fire perimeter $X^{\mu}(k+1)$ with the covariance at each point is summarized in Fig. 3.

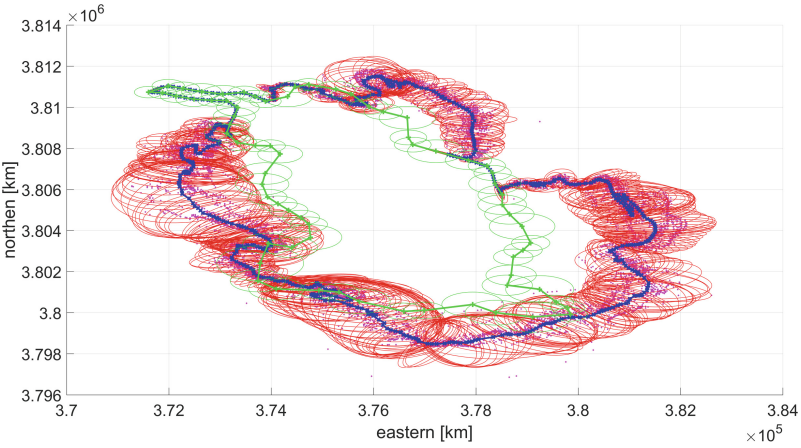

Fig. 3. Comparison of the mean (blue) and variance (red) of the ensemble forward simulation and measured fire perimeter (green) *before* the data assimilation at time step $k+1$. (Color figure online)

From Fig. 3 one may recognize the stationary points for the fire perimeter at time step $k = 1$ indicated earlier in Fig. 2. In addition, it can be observed (especially in the bottom right of the graph) that the ensemble forward simulation results may be biased and may have an incorrectly estimated covariance compared to the measurements. It is clear that the forward simulations require a data assimilation step to provide a better fit to the measured fire perimeter $Y(k+1)$ and adjust the covariance information.

Application of the data assimilation procedure outlined earlier in Sect. 3.2 now leads to a correction on both the mean and covariance of the predicted fire perimeter $X(k+1)$ at the time step $k+1 = 2$. The results are summarized in

Fig. 4 where it can be observed that the ensemble Kalman filter adjusted forward simulation now provides a much better fit to the measured fire perimeter at the next time step $k+1$.

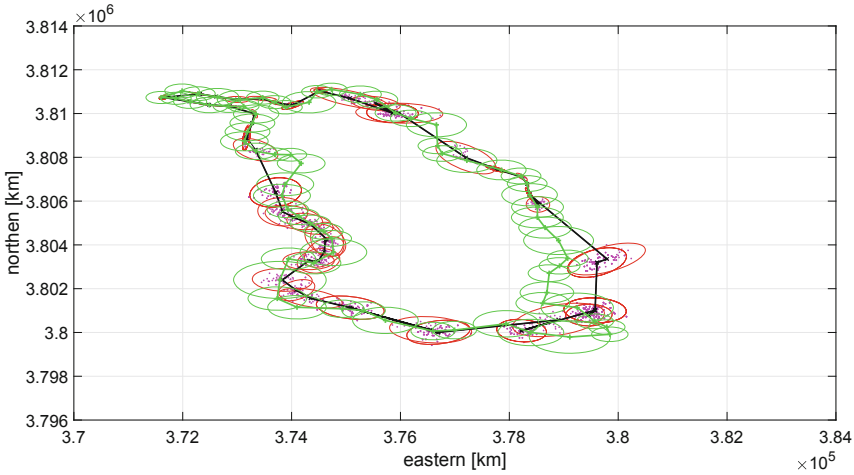

Fig. 4. Comparison of mean value (black) and variance (red) of Kalman filtered updated fire perimeter and measured fire perimeter (green) *after* the data assimilation at step $k+1$. (Color figure online)

4.2 Definition of Fire Coverage Error

For the evaluation of the performance and improvement of wildfire data assimilation it is important to carefully characterize the error between two fire perimeters. Typically, the error is computed using the euclidean distance between points in a predicted fire perimeter and points along the measured fire perimeter [17]. This method is not suitable in large scale fires as the number of points along a fire perimeter can be vastly different in the predicted and the measured fire perimeter. Instead, we define the error using lower and upper bounds on the surface of the overlapping area of the fire perimeter, taking into accounts the uncertainty or variability of the fire perimeters.

Figure 5 has a visual illustration of how the error and its lower and upper bounds are computed. All points along the fire perimeter are associated with a value of uncertainty for the predicted fire perimeter and the measured fire perimeter. The uncertainty is represented in the form of an ellipse, which represents the confidence interval of where that particular point could lie. For the computation of the lower and upper bounds, we compute the area A_p covered by the predicted fire perimeter and the area A_m covered by the measured fire perimeter. Based on these areas, the mean value of the fire coverage error A_e is computed via

$$A_e = A_p \cup A_m - 2(A_p \cap A_m) \tag{7}$$

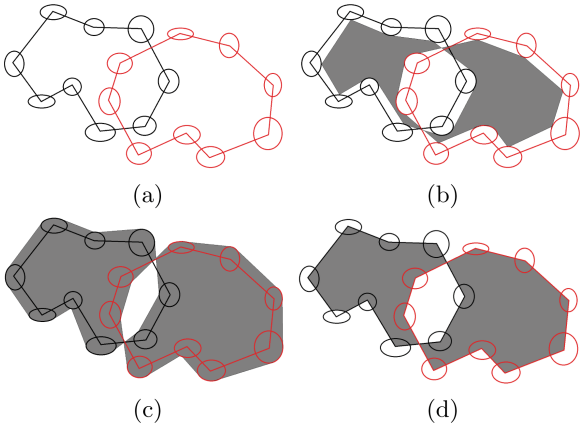

Fig. 5. (a) Predicted fire perimeter (black) and measured fire perimeter (red), grey area in (b): minimum error in area coverage (lower bound on error uncertainty), (c): maximum error in area coverage (upper bound on error uncertainty) and (d): mean error in area coverage. (Color figure online)

whereas lower and upper bounds are created by taking into account the variability or uncertainty on each fire perimeter.

4.3 Performance Comparison of Data Assimilation with Barrier Points

The single step data assimilation summarized earlier in Fig. 4 illustrates an improvement in the fire coverage error. The question remains whether the identification of stationary points and used as barrier points in FARSITE indeed improves the fire coverage error, in addition to improvements achieved by standard ensemble Kalman filter based data assimilation techniques. To illustrate the improvement of the fire coverage error, the subsequent steps of ensemble forward simulation and data assimilation for several time step $k = 0, 1, \ldots, 4$ is performed *with* and *without* the identification of stationary points.

To summarize the improvement in performance, the mean value of the fire coverage error A_e as defined in (7) along with the upper and lower bounds due to the variability on the fire perimeters is computer for the different time steps. The results are summarized in Fig. 6 and the improvement in performance measured in fire coverage error is evident from the graph. Both uncertainty and magnitude of the fire coverage error have been reduced when data assimilation is performed, but results are further improved when stationary points are identified and used as barrier points in the ensemble forward simulations. Especially the upper bound on the fire coverage error remains at acceptable levels during several data assimilation steps when using the identified stationary points on the fire perimeter.

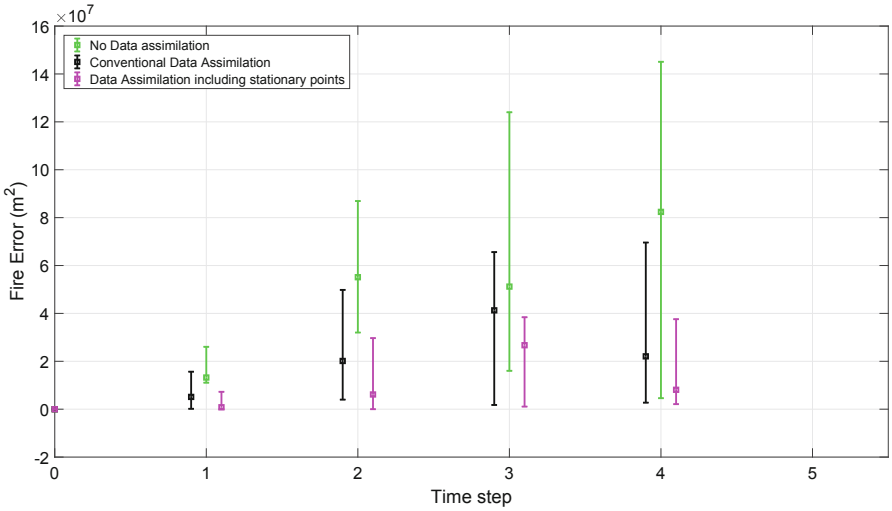

Fig. 6. Mean value, lower bounds and upper bounds on the fire coverage error A_e as defined in (7) for: no data assimilation (green), ensemble Kalman filtering *without* stationary points (black) and ensemble Kalman filtering *with* identification of stationary points (magenta). (Color figure online)

5 Conclusions

This papers shows the importance of data assimilation combined with the identification of stationary points in correcting the prediction of the spread of wildfires at a large scale. Stationary points are identified by comparison of subsequent fire perimeters and used in FARSITE to define barrier points to limit fire propagation. Based on the observations of the 2016 Sandfire, it is shown that the combined use of data assimilation and barrier points can significantly improve the fire coverage error. It is worth noting that an Ensemble Kalman Filter (EKF) approach is used to perform data assimilation, where a Gaussian representation of the fire perimeter vector is assumed. However, in certain situations it would be more suitable to implement a particle filter to take into account non-Gaussian distributions of fire perimeter uncertainty for future research directions.

References

1. Artés, T., Cencerrado, A., Cortés, A., Margalef, T.: Relieving the effects of uncertainty in forest fire spread prediction by hybrid MPI-OpenMP parallel strategies. Procedia Comput. Sci. **18**, 2278–2287 (2013)
2. Mandel, J., Beezley, J.D.: An ensemble Kalman-particle predictor-corrector filter for non-Gaussian data assimilation. In: Allen, G., Nabrzyski, J., Seidel, E., van Albada, G.D., Dongarra, J., Sloot, P.M.A. (eds.) ICCS 2009. LNCS, vol. 5545, pp. 470–478. Springer, Heidelberg (2009). https://doi.org/10.1007/978-3-642-01973-9_53

3. Cheney, N., Gould, J., Catchpole, W.: The influence of fuel, weather and fire shape variables on fire-spread in grasslands. Int. J. Wildland Fire **3**(1), 31–44 (1993)
4. Evensen, G.: Data Assimilation: The Ensemble Kalman Filter. Springer-Verlag, Heidelberg (2009). https://doi.org/10.1007/978-3-642-03711-5
5. Fang, M., Srivas, T., de Callafon, R., Haile, M.: Ensemble-based simultaneous input and state estimation for nonlinear dynamic systems with application to wildfire data assimilation. Control Eng. Pract. **63**, 104–115 (2017)
6. Filippi, J.B., Pialat, X., Clements, C.: Assessment of ForeFire/Meso-NH for wildland fire/atmosphere coupled simulation of the FireFlux experiment. Proc. Combust. Inst. **34**(2), 2633–2640 (2013)
7. Finney, M.: FARSITE: fire area simulator-model development and evaluation. Technical report RMRS-RP-4 Revised, U.S. Department of Agriculture, Forest Service, Rocky Mountain Research Station (2004)
8. Gillijns, S., Mendoza, O., Chandrasekar, J., De Moor, B., Bernstein, D., Ridley, A.: What is the ensemble Kalman filter and how well does it work? In: American Control Conference, Minneapolis, MN, pp. 4448–4453 (2006). https://doi.org/10.1109/ACC.2006.1657419
9. Khul, F., Giardina, C.: Elliptical Fourier features of a closed contour. Comput. Graphics Image Process. **18**, 236–258 (1982)
10. Mandel, J., Beezley, J., Cobb, L., Krishnamurthy, A.: Data driven computing by the morphing fast Fourier transform ensemble Kalman filter in epidemic spread simulations. Procedia Comput. Sci. **1**, 1221–1229 (2010)
11. Mandel, J., et al.: Towards a dynamic data driven application system for wildfire simulation. In: Sunderam, V.S., van Albada, G.D., Sloot, P.M.A., Dongarra, J.J. (eds.) ICCS 2005. LNCS, vol. 3515, pp. 632–639. Springer, Heidelberg (2005). https://doi.org/10.1007/11428848_82
12. Mandel, J., et al.: A note on dynamic data driven wildfire modeling. In: Bubak, M., van Albada, G.D., Sloot, P.M.A., Dongarra, J. (eds.) ICCS 2004. LNCS, vol. 3038, pp. 725–731. Springer, Heidelberg (2004). https://doi.org/10.1007/978-3-540-24688-6_94
13. Oriol, R., Miguel, V., Elsa, P., Planas, E.: Data-driven fire spread simulator: validation in Vall-llobrega's fire. Front. Mech. Eng. **5**, 1–11 (2019)
14. Rochoux, M., Ricci, S., Lucor, D., Cuenot, B., Trouvé, A., Bart, J.: Towards predictive simulations of wildfire spread using a reduced-cost ensemble Kalman filter based on polynomial chaos approximations. In: Proceedings of the Summer Program, Center for Turbulence Research (2012)
15. Simon, D.: Kalman filtering with state constraints: a survey of linear and nonlinear algorithms. IET Control Theory Appl. **4**(8), 1303–1318 (2010)
16. Srivas, T., Artés, T., de Callafon, R., Altintas, I.: Wildfire spread prediction and assimilation for FARSITE using ensemble Kalman filtering. Procedia Comput. Sci. **80**, 897–908 (2016)
17. Zhang, C., Rochoux, M., Tang, W., Gollner, M., Filippi, J.B., Trouvé, A.: Evaluation of a data-driven wildland fire spread forecast model with spatially-distributed parameter estimation in simulations of the FireFlux I field-scale experiment. Fire Saf. J. **91**, 758–767 (2017)